Check for updates

Fast and non-destructive Raman spectroscopic determination of multi-walled carbon nanotube (MWCNT) contents in MWCNT/polydimethylsiloxane composites†

Donghyun Ryoo,‡ Jong Yun Kim,‡ Pham Khac Duy, Sang Hoon Cho, Hoeil Chung [ID] * and Tae Hyun Yoon [ID] *

A versatile Raman spectroscopic method to determine the contents of carbon nanotubes (CNTs) in CNT/polydimethylsiloxane (PDMS) composites is demonstrated, and important issues directly related to the accuracy of the measurement have been investigated. Initially, Raman microscopic mappings over an area of 6.0×6.0 mm^2 were carried out on CNT/PDMS composites, which revealed the existence of the partial localization of CNTs on a microscopic scale. Therefore, a laser illumination scheme covering a large sample area of 28.3 mm^2 was employed to acquire a sample spectrum representative of the whole CNT concentration. The peak area ratio between the CNT and PDMS peaks clearly varied with the CNT concentration, whereas the reproducibility of measurements was degraded for the composites containing more than 3.0 wt% CNTs because of the decreased Raman sampling volume arising from the absorption of laser radiation by the CNTs. The laser penetration depth was semi-quantitatively investigated by observing the spectra of thin-sliced samples collected by positioning a Teflon disk behind the sample, and Monte Carlo simulations were employed to examine the internal photon propagation as well as explain the experimental observation. In summary, the fundamental issues affecting the Raman measurement of the CNT containing polymer matrix have been clearly addressed, and the finding here will be a beneficial basis for successful Raman spectroscopic analysis of different CNT-containing composites.

Introduction

Carbon nanotubes (CNTs) have been utilized as versatile nanofillers for multifunctional polymer nanocomposites because of their unique electronic, thermal, optical, mechanical, and chemical properties.[1–8] Therefore, CNT/polymer nanocomposites with enhanced material functionality are being widely used in diverse commercial products such as sporting goods, packaging, and electronic devices.[9,10] However, CNTs could have a harmful effect on human health, as well as the environment, when they are released from the products.[11–20] Therefore, health and safety concerns over CNT-containing consumer products have increased. In this context, the determination of CNT concentrations in various composite samples

Department of Chemistry and Research Institute for Convergence of Basic Sciences, Hanyang University, Seoul 133-791, Republic of Korea. E-mail: hoeil@hanyang.ac.kr, taeyoon@hanyang.ac.kr; Fax: +82-2-2299-0762; Tel: +82-2-2220-0937, +82-2-2220-4593

†Electronic supplementary information (ESI) available. See DOI: 10.1039/c8an00351c

‡Equal contribution authors.

becomes essential for the safety regulation of CNT-containing products, as well as their risk assessment. Regarding the determination of CNT contents in samples, several investigations have been reported, such as the measurement of suspended CNT fractions using electron paramagnetic resonance (EPR),[21] the quantification of the fractions of mixed and dispersed carbon nanotubes using Raman spectroscopy,[22] the quantitative assessment of CNT dispersions using scanning electron microscopy (SEM) images[23] and Raman spectroscopy,[24] and the determination of CNT concentrations in aqueous dispersions using UV-visible spectroscopy.[25] These studies have mainly analyzed dispersed CNTs in liquid media by employing various analytical methods; however, no study has attempted to directly determine the CNT content of CNT-embedded solid composites in a non-destructive manner.

Raman spectroscopy is a suitable candidate for this task because of the distinct Raman peaks of CNTs that correspond to the disorder (D) and graphite peaks (G) and the measurements are non-destructive. Thus, Raman spectroscopy is frequently used for analyzing CNTs present in mixtures, such as a polymer/CNT or a metal/CNT[5,26,27] and studying the physicochemical properties of CNTs based on their D/G peak ratios,

as well as peak shifts.[28] As described, the use of Raman spectroscopy could enable the determination of CNT contents in polymer composites; however, some critical issues must be addressed for accurate analysis. The first is the distribution homogeneity of CNTs in the sample. Because a dispersion of CNTs in a polymer is not homogeneous on a microscopic scale, the obtained Raman spectrum may not quantitatively represent the whole CNT concentration of a sample when the sampling volume is small. The second is the strong absorption of laser radiation by the black-colored CNTs, which limits the diffusion of laser photons into a sample. Thus, the sample interrogation volume in Raman measurement is limited, potentially reducing the reproducibility of Raman measurements. The investigation and provision of answers on these issues, further versatile for quantitative analysis of CNTs in diverse polymer composites, were the main motivation for this study.

With these issues in mind, CNT/polydimethylsiloxane (PDMS) composites with varying CNT concentrations (0.5–5.0 wt%) were prepared, and the CNT concentrations were determined using Raman spectroscopy. Initially, Raman mapping was performed over an area of 6.0×6.0 mm^2 on the composites, and the microscopic distribution homogeneity of the CNTs was examined. Subsequently, to acquire spectra that were more representative of the whole CNT concentration by considering the occasional localization of CNTs in the samples, a wide area illumination (WAI) scheme covering a large sampling area of 28.3 mm^2 (laser illumination diameter: 6 mm) was employed. The spectral features of CNT and PDMS components were characterized, and then the peak area ratios between both peaks were correlated with the CNT concentrations. The resulting accuracy and concentration-dependent reproducibility of the measurements were also assessed because the depth of laser diffusion in a sample was expected to be dependent on the CNT concentration because of the absorption of laser radiation by the CNTs. To semi-quantitatively investigate the dependence of the penetration depth on the CNT concentration, Raman spectra of slices of the composites (thickness: 1 mm) with different CNT concentrations were collected by positioning a Teflon disk behind the sample. If Teflon peaks were observed in the collected spectra, it indicated that the laser photons had passed through the 1 mm-thick sample slices. Finally, Monte Carlo simulations[29,30] were performed to investigate the distributions of Raman photons in the sliced samples and explain the experimental observations.

Experimental section

Preparation of CNT/PDMS composite samples

PDMS (Sylgard 184 kit, Dow Corning Corporation) and multi-walled carbon nanotubes (MWCNTs) with an outer diameter of ~19 nm (CM-100 & C-091204-3, Hanwha Chemical Co., Korea) were used to fabricate the CNT/PDMS nanocomposite samples. Initially, the PDMS curing agent and the PDMS base

were mixed at a weight ratio of 1 : 10. Then, the CNTs were added to the mixed matrix and vigorously blended until uniform dispersions of CNTs were confirmed by visual observation. The mixture was placed in an oven for 2 h at 60 °C for degassing and then cured after drop casting and leveling on a Petri dish. Ten samples with varying CNT concentrations (0.5–5.0 wt% with an interval of 0.5 wt%) were prepared. The thicknesses of the samples were approximately 10.0 mm. Pictures of some selected CNT/PDMS composite samples are shown in the ESI.†

### Acquisition of Raman spectra and Monte Carlo simulations

To acquire the Raman spectra, the WAI scheme (PhAT system, Kaiser Optical Systems, USA) using circular laser (785 nm) illumination (diameter: 6 mm) to cover a large sample area (28.3 mm^2) with a long focal length (≈25 cm) was used. The CNT/PDMS composite sample was located at the focal point of laser illumination for the collection of the spectra. Each Raman spectrum (resolution: 4 cm^{-1}) was obtained by accumulating 150 scans with a 2 s exposure (laser power: 400 mW). To examine the homogeneity of CNT distribution, Raman mapping was performed on the surface of the CNT/PDMS composite sample. The sample was positioned on a microscope stage connected to a Raman spectrometer (Kaiser Optical Systems), and the laser was focused using an objective lens (10 × 0.25 numerical aperture (NA)) to collect the Raman spectra. The laser spot size was approximately 100 μm in diameter and the laser power was maintained at 20 mW. Each Raman spectrum (resolution: 4 cm^{-1}) was obtained by accumulating 75 scans with a 2 s exposure during mapping. The baseline correction of the spectra, the calculation of the peak area, and quadratic curve fitting to find the relationship between the peak area ratio and CNT concentration were performed using MATLAB version 7.0 (Mathworks Inc., MA, USA).

The Monte Carlo simulation package developed by F. F. De Mul[29,30] was used in this study. The parameters used for the simulation, such as the absorption coefficient and reduced scattering coefficient, are summarized in the ESI,† and a detailed description of the simulation parameters can be found in previous publications.[31–33] The number of illuminated laser photons was 100 000, and the laser photons were homogeneously distributed over the illumination area. The diameters of the illumination area and the detection window input for the simulation were equal to the experimental values.

Results and discussion

Examination of distribution homogeneity of CNTs in CNT/PDMS composite samples

The Raman spectra of pure PDMS and MWCNTs (hereinafter referred to as CNTs) in the 1750–1150 cm^{-1} range are shown at the top of Fig. 1. Because the Raman intensities of CNTs are approximately 45 times lower than those of PDMS, the CNT spectrum is magnified at the bottom for detailed examination.
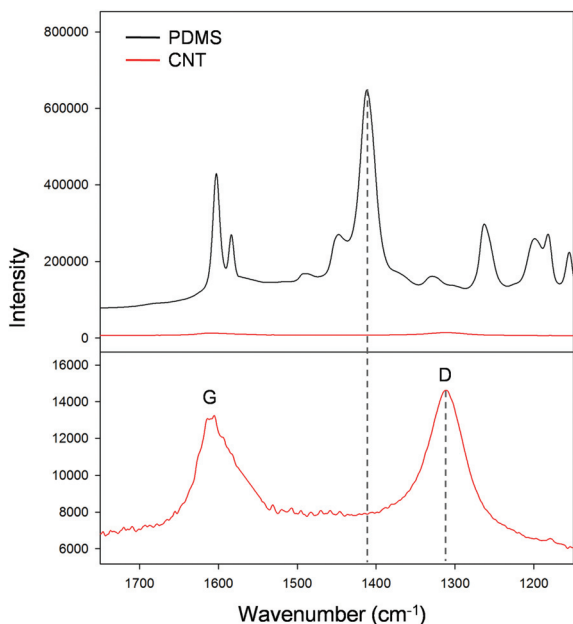
Fig. 1 Raman spectra of pure PDMS and CNTs in the 1750–1150 cm^{-1} range (top). The CNT spectrum is magnified at the bottom, indicating the G and D bands.

As is shown, the G band at 1611 cm^{-1} and the D band at 1316 cm^{-1} originated from the Raman-active in-plane atomic displacement E_{2g} mode and disorder-induced features of CNTs, respectively, are clearly observable.[26,27,34] The G band greatly overlaps with two PDMS peaks located at 1583 and 1602 cm^{-1}, whereas the D band is much less overlapped with the nearby PDMS peaks. Therefore, the D band is more useful for the determination of the CNT concentration and the PDMS peaks are expected to be dominant in the sample spectra because the CNT concentration is much lower, that is, below 5.0 wt%.

Although the homogeneous dispersion of CNTs in a liquid polymer phase is probably achievable, the dispersion in the final solid composite would not be homogeneous on a microscopic scale. Therefore, to investigate the microscopic distribution homogeneity of CNTs in the CNT/PDMS composite, Raman mapping was separately performed using both 0.5 and 5.0 wt% CNT samples. The mapping intervals were 250 and 250 μm in the x- and y-directions, respectively, and a total of 576 spectra (24 points per mapping line, and a total of 24 line mappings) was collected over an area of 6 × 6 mm^2 over 24 hours. Fig. 2(a) shows a Raman mapping image of the 0.5 wt% sample constructed using the peak intensity of the D band. The baselines of the spectra were corrected at 1780, 950, and 300 cm^{-1} before the construction of the image.

The distributions of yellow/red (higher intensity) and blue (lower intensity) colors in the image are somewhat homogeneous; however, the CNTs seem to be more localized at the bottom and the top left. In the case of the 5.0 wt% sample (Fig. 2(b)), the localization of CNTs at the bottom is more severe because of the higher CNT content. Based on the exam-
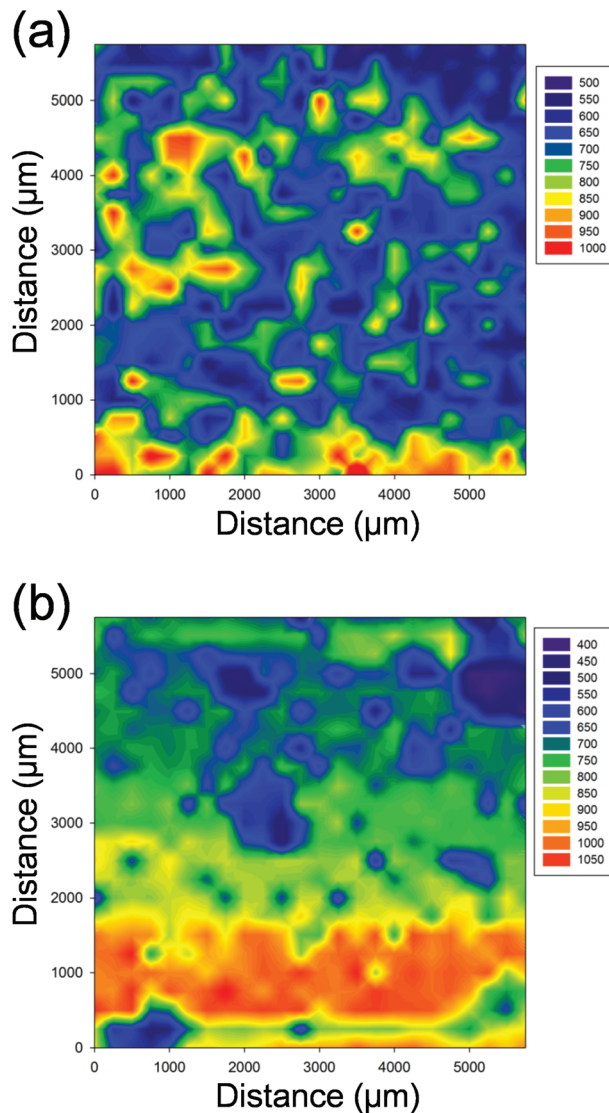

Fig. 2 Raman mapping images separately acquired from the 0.5 (a) and 5.0 wt% (b) CNT/PDMS composite samples. The mapping intervals were 250 and 250 μm in the x and y-directions, respectively, and a total of 576 spectra was collected over the area of 6 × 6 mm^2. The image was constructed using the peak intensity of the D band at 1316 cm^{-1}.

ination of the two mapping images, the partial localization of CNTs in the samples clearly occurs and becomes more apparent as the CNT concentration increases. This finding indicates that, to obtain spectra representative of the whole CNT concentration, laser radiation on a large sample area in spectral acquisition is required. Thus, for the accurate determination of the CNT concentration, the WAI scheme is a versatile choice.

Examination of sample spectral features with varying CNT concentrations

Fig. 3(a) shows the Raman spectra of the CNT/PDMS composite samples with five different CNT concentrations (0.5, 1.0, 2.0, 3.5, and 5.0 wt%) collected using the WAI scheme. One
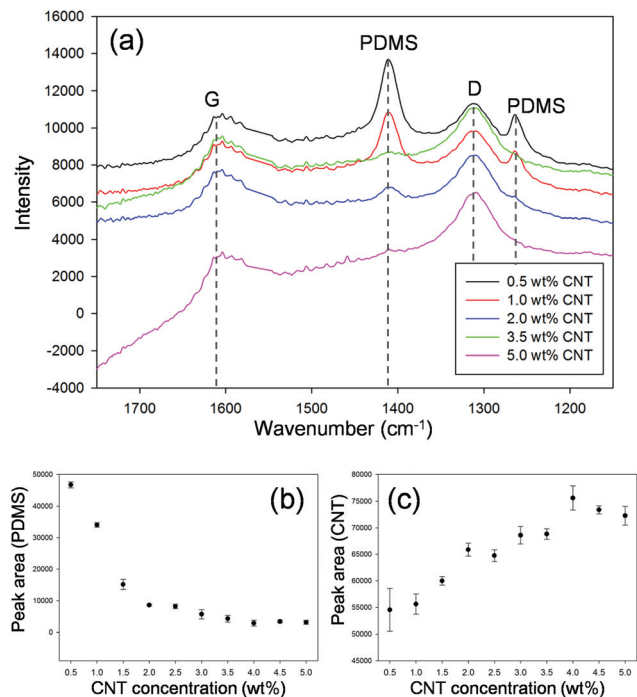
Fig. 3 Raman spectra of the CNT/PDMS composite samples with five different CNT concentrations (0.5, 1.0, 2.0, 3.5, and 5.0 wt%) collected using the WAI scheme (a). The peak areas of the PDMS band at 1412 cm^{-1} (b) and the D band (c) are plotted against the CNT concentrations.

notable observation here is that the intensity of the PDMS bands, such as the strongest 1412 cm^{-1} band originating from CH_3 asymmetric bending,[35] is surprisingly lower than that expected; the PDMS peaks should be dominant because of the high concentration. The low PDMS peak intensity is mainly attributed to the strong absorption of laser radiation by the black-colored CNTs. When laser photons hit the CNT, a large portion of photons are absorbed, and only a small portion of unabsorbed photons reach PDMS for interaction. Therefore, the chances of laser photons interacting with PDMS are substantially diminished, resulting in the low PDMS peak intensity. As shown, both CNT and PDMS peaks are present until the CNT concentration reaches 2.0 wt%. At higher CNT concentrations (3.5 and 5.0 wt%), the PDMS peaks almost disappear because of the larger attenuation of laser photons and the re-absorption of the generated PDMS Raman photons because of the high content of CNTs.

For the quantitative investigation of the intensity variation, the peak areas of the PDMS band at 1412 cm^{-1} and the D band are plotted against the CNT concentrations in Fig. 3(b) and (c), respectively. The error bars were calculated based on five replicate measurements of each sample. The laser was randomly irradiated on different locations on the sample for the replicate measurements. The reduction in the PDMS peak with increasing CNT concentration is exponential rather than linear. This means that the number of Raman photons generated from PDMS that reach the detector decreases more sub-

stantially as the CNT concentration increases. In addition, the peak area of CNTs increases with increasing concentration, up to 4.0 wt%; however, no correlation with the concentration was observed for high concentrations. It seems that the re-absorption of generated CNT Raman photons by neighbouring CNTs becomes significant when the concentration is greater than 4.0 wt%. Based on the above plots, the use of the absolute CNT intensity for concentration determination is not sufficiently accurate.

Because the attenuation of the PDMS as well as CNT Raman photons occurs concurrently, the use of the peak area ratio between the CNT and PDMS peaks would more correctly follow the concentration variation. In addition, the peak area ratio method is more versatile for Raman-based quantitative analysis because it effectively compensates for the fluctuation in peak intensities induced by unwanted sources such as variations in the laser power and sample morphology. Thus, the peak area ratio was obtained by dividing the area of the D band by the area of the PDMS band at 1412 cm^{-1} for each sample, and the correlation between the peak ratio and CNT concentration was examined and is shown in Fig. 4. The peak area ratio clearly increases with increasing CNT concentration, and the trend is slightly non-linear. The 4.0 wt% sample was excluded as an outlier based on the t-test because its peak area ratio was substantially higher compared to those of the neighbouring samples. A regression line, $y = 0.27x^2 + 4.00x - 1.93$, through the data points was obtained from quadratic curve fitting, and the resulting R^2 is 0.983. The peak area ratio quite accurately follows the variation of the CNT concentration. However, when the 4.0 wt% sample was included, R^2 fell to 0.885.

Evaluation of laser penetration depths in CNT/PDMS composite samples

The most noticeable observation in the correlation plot in Fig. 4 is that the reproducibility of replicate measurements becomes significantly worse for the samples containing a CNT
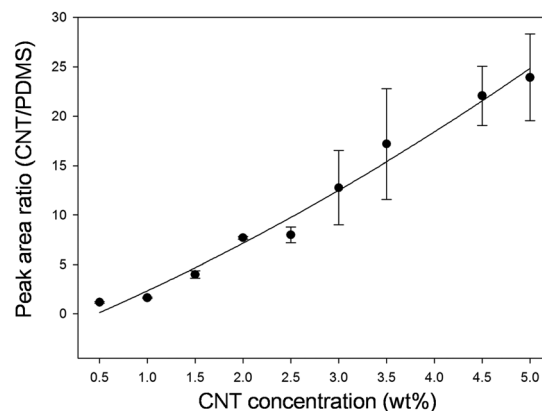
Fig. 4 Correlation between the peak area ratio (CNT/PDMS) and CNT concentration in the Raman measurements of the composite samples. The peak area ratio was obtained by dividing the area of the D band by the area of the PDMS band at 1412 cm^{-1} for each sample.

loading of more than 3.0 wt%. This observation clearly demonstrates that a larger amount of CNTs reduces the reproducibility of the measurements and degrades the accuracy. To probe the potential causes of the degradation, we evaluated the laser penetration depth governing the Raman sampling volume semi-quantitatively. For this purpose, some of the CNT/PDMS composites were cut into 1 mm-thick slices, and their back-scattering Raman spectra were collected by positioning Teflon blocks behind the samples. Fig. 5(b) shows the Raman spectra in the 1450–1150 cm^{-1} region of the 1 mm-thick 0.5 wt%, 2 mm-thick 0.5 wt%, 1 mm-thick 2.5 wt%, and 1 mm-thick 5.0 wt% samples collected in the described way. In the identical region, incorporation of the main three Teflon peaks and D band is highlighted, and the Raman spectrum of the Teflon block is shown in Fig. 5(a). In the case of the 1 mm-thick 0.5 wt% sample, the Teflon peak at 1380 cm^{-1} is present along with the PDMS peaks. This indicates that a certain population of laser photons crosses the 1 mm-thick sample barrier and the generated Teflon Raman photons can travel back to the detector through the slice. When the thickness of the 0.5 wt% sample was increased to 2 mm, the Teflon peak disappeared. Thus, photons are unable to reach the Teflon block through the corresponding slice, or the generated Teflon Raman photons cannot cross the barrier to reach the detector. In the cases of the 1 mm-thick 2.5 wt% and 1 mm-thick 5.0 wt% samples, the Teflon peaks were not observed. The higher CNT concentrations probably prevent the laser photons from reaching the Teflon block.

Overall, the observations indicate that the sampling depth could be around 1.0–1.5 mm when the CNT concentration is less than 2.0 wt% but becomes significantly shallower for composite samples with more than 2.0 wt% CNTs. Thinner slices are preferable for more precise estimation, but it was difficult to prepare the slices with a thickness below 1.0 mm mechanically. Nonetheless, the observation clearly demonstrates that the sample interrogation volume in the Raman measurement of high-concentration samples is small. Therefore, the decreased sampling volume makes the acquired spectra less

representative of the concentration because the partial localization of CNTs becomes more evident for high-concentration samples such as the 5.0 wt% CNT sample, as shown in Fig. 2, and the larger variation in the peak area ratio in the replicate measurements is a consequence.

To visualize the distributions of Raman photons in the samples, Monte Carlo simulations,[29,30] a powerful method for studying photon migration in a solid sample, were employed. The parameters used for the simulations are summarized in the ESI,† as described. Fig. 6 shows the side-views of all generated Raman photons from CNTs, PDMS, and Teflon (left) in the 1 mm-thick 0.5 wt% (a), 2 mm-thick 0.5 wt% (b), 1 mm-thick 2.5 wt%, (c) and 1 mm-thick 5.0 wt% (d) samples, when the Teflon block is positioned behind each sample. The left and right layer indicates the sample and Teflon block, respectively. The laser irradiated the samples from the left, and the dots indicate the spatial locations of the Raman photons. In addition, the number of Raman photons distributed along the depth profile is displayed at the right of the corresponding side-view. The black, red, blue, and pink colors correspond to the total, CNT, PDMS, and Teflon Raman photons, respectively. In the case of the 1 mm-thick 0.5 wt% sample, a substantial number of Teflon Raman photons were generated in the far-left layer of Teflon. This indicates that sufficient numbers of laser photons crossed the sample and interacted with Teflon.

Then, the generated Teflon Raman photons are able to traverse the same medium for detection. In the case of the 2 mm-thick 0.5 wt% sample, the number of generated Teflon Raman photons decreased significantly (by approximately 5 times) in comparison with that of the 1 mm-thick sample because of the larger attenuation of laser photons by the increased (doubled) thickness. These generated Teflon photons were then mostly absorbed by CNTs during the journey to the detector; thus, no Teflon peak was observed in the experimentally acquired spectrum, as shown in Fig. 5. When the photon distributions in the 1 mm-thick 2.5 and 5.0 wt% samples are examined, no Teflon Raman photons are generated, although the sample
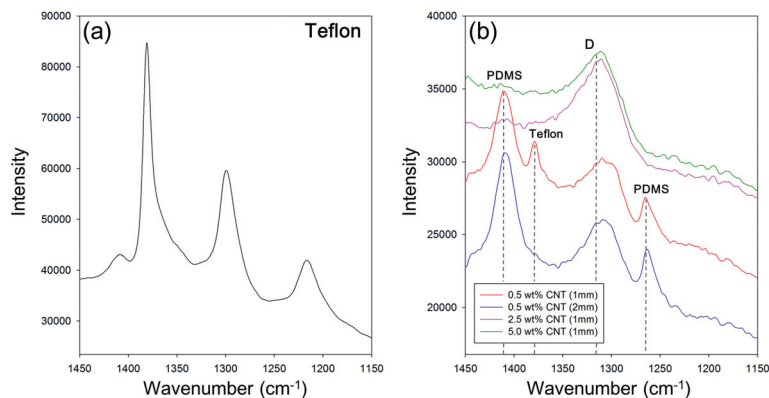
Fig. 5 Raman spectrum of the Teflon block in the 1450−1150 cm^{-1} region (a). There are 3 major peaks located at 1381, 1298, and 1214 cm^{-1}, respectively. Raman spectra of the 1 mm-thick 0.5 wt%, 2 mm-thick 0.5 wt%, 1 mm-thick 2.5 wt%, and 1 mm-thick 5.0 wt% samples collected by positioning the Teflon disk behind the samples are shown (b). The dashed lines indicate the positions of the respective Raman peaks.
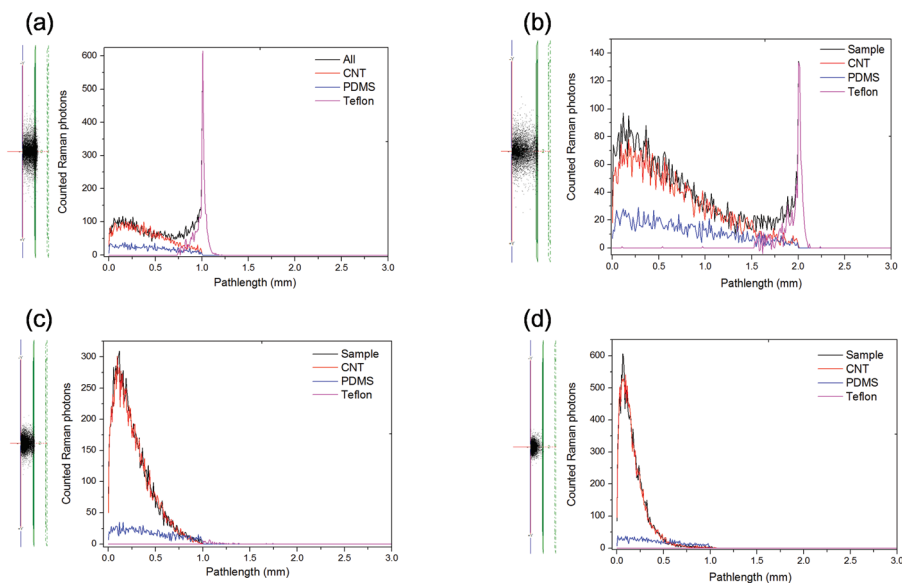
Fig. 6 Side-views of all generated Raman photons from CNTs, PDMS, and Teflon (left) in the 1 mm-thick 0.5 wt% (a), 2 mm-thick 0.5 wt% (b), 1 mm-thick 2.5 wt% (c), and 1 mm-thick 5.0 wt% (d) samples, when the Teflon block is placed behind each sample. The left and right layer indicates the sample and Teflon block, respectively. The laser irradiated the samples from the left. In addition, the number of Raman photons distributed along the depth profile is displayed at the right of the corresponding side-view.

thickness is still 1 mm. Thus, the increase in the CNT concentration results in the laser photons being unreachable to the Teflon located behind the sample. Overall, the simulation results agree well with the experimental observations in Fig. 5.

When the CNT photons in the 1 mm-thick 0.5, 2.5, and 5.0 wt% samples are compared (Fig. 6(a), (c), and (d)), the distribution becomes narrower, and the location of the nominal population moves closer to the sample surface as the CNT concentration increases. In the case of the 2.5 wt% sample, the CNT photons are narrowly populated around a depth of 0.12 mm, and the nominal penetration depth in the 5.0 wt% sample is closer to the surface. Thus, near-surface sampling is only possible in the case of the 5.0 wt% sample. In addition, the photon distribution in the side-views becomes smaller with increasing CNT concentration. The simulation clearly indicates that the Raman sampling volume decreases significantly in the measurements of high-concentration samples and the reduced sampling volume degrades the measurement reproducibility, especially when the localization of CNTs in a sample is more severe. In addition, the simulation also correctly predicts the generation of a much lower number of PDMS Raman photons, although PDMS is the dominant component.

Conclusion

Based on the results of this study, Raman spectroscopy is an appropriate analytical method for the non-destructive determination of the total CNT concentration in CNT/PDMS composites as well as other CNT-incorporated polymers such as CNT/polyethylene and CNT/polyurethane. Other non-destructive

methods, such as absorption-based infrared (IR) and near-infrared (NIR) spectroscopy, could be used; however, these methods are applicable only for the analysis of thin composite films because of the strong IR/NIR absorption of CNTs. The WAI scheme, which provides a large sampling area, was helpful in correctly representing the CNT concentration in the Raman spectra of the tested samples, in which the penetration (diffusion) depth of laser radiation was considerably limited by the strong photon absorption of CNTs. Nonetheless, the reproducibility of measurement must be improved for more accurate analysis. To meet this goal, a fast hyperspectral Raman imaging method able to cover the whole sample surface or the use of a NIR laser with deep axial penetration into the sample for spectral acquisition are possible alternatives, and these investigations are underway in our research group. Finally, when Raman spectroscopy is utilized to determine the CNT concentration in many different CNT-containing composites, the distribution homogeneity of CNTs and the actual laser sampling volume in a given sample should be investigated, and we hope that this publication will act as a basis for future related studies.

Conflicts of interest

There are no conflicts to declare.

Acknowledgements

References

1 F. Du, J. E. Fischer and K. I. Winey, *Phys. Rev. B*, 2005, **72**, 121404(R).

2 C. A. Dyke and J. M. Tour, *J. Phys. Chem. A*, 2004, **108**, 11151–11159.

3 H. Huang, C. H. Liu, Y. Wu and S. Fan, *Adv. Mater.*, 2005, **17**, 1652–1656.

4 T. Kashiwagi, F. Du, J. F. Douglas, K. I. Winey, R. H. Harris Jr. and J. R. Shields, *Nat. Mater.*, 2005, **4**, 928–933.

5 A. Martinez, S. Uchida, Y. W. Song, T. Ishigure and S. Yamashita, *Opt. Express*, 2008, **16**, 11337–11343.

6 M. Moniruzzaman and K. I. Winey, *Macromolecules*, 2006, **39**, 5194–5205.

7 R. Ramasubramaniam, J. Chen and H. Liu, *Appl. Phys. Lett.*, 2003, **83**, 2928–2930.

8 B. Vigolo, A. Penicaud, C. Coulon, C. Sauder, R. Pailler, C. Journet, P. Bernier and P. Poulin, *Science*, 2000, **290**, 1331–1334.

9 J. S. Mohan Raja, *Carbon Nanotubes and Their Applications*, 2014.

10 M. F. De Volder, S. H. Tawfick, R. H. Baughman and A. J. Hart, *Science*, 2013, **339**, 535–539.

11 P. Cherukuri, S. M. Bachilo, S. H. Litovsky and R. B. Weisman, *J. Am. Chem. Soc.*, 2004, **126**, 15638–15639.

12 S. Fiorito, A. Serafino, F. Andreola and P. Bernier, *Carbon*, 2006, **44**, 1100–1105.

13 M. Geiser, B. Rothen-Rutishauser, N. Kapp, S. Schürch, W. Kreyling, H. Schulz, M. Semmler, V. I. Hof, J. Heyder and P. Gehr, *Environ. Health Perspect.*, 2005, **113**, 1555–1560.

14 H. Grubek-Jaworska, P. Nejman, K. Czumińska, T. Przybyłowski, A. Huczko, H. Lange, M. Bystrzejewski, P. Baranowski and R. Chazan, *Carbon*, 2006, **44**, 1057–1063.

15 J. C. H. Cheng, *Off. J. Soc. Toxicol.*, 2005, **84**, 9.

16 A. Huczko and H. Lange, *Fullerene Sci. Technol.*, 2001, **9**, 247–250.

17 A. Huczko, H. Lange, M. Bystrzejewski, P. Baranowski, H. Grubek-Jaworska, P. Nejman, T. Przybyłowski, K. Czumińska, J. Glapiński, D. R. M. Walton and H. W. Kroto, *Fullerenes, Nanotubes, Carbon Nanostruct.*, 2005, **13**, 141–145.

18 G. Jia, H. Wang, L. Yan, X. Wang, R. Pei, T. Yan, Y. Zhao and X. Guo, *Environ. Sci. Technol.*, 2005, **39**, 1378–1383.

19 V. E. Kagan, Y. Y. Tyurina, V. A. Tyurin, N. V. Konduru, A. I. Potapovich, A. N. Osipov, E. R. Kisin, D. Schwegler-Berry, R. Mercer, V. Castranova and A. A. Shvedova, *Toxicol. Lett.*, 2006, **165**, 88–100.

20 J. Muller, F. Huaux, N. Moreau, P. Misson, J. F. Heilier, M. Delos, M. Arras, A. Fonseca, J. B. Nagy and D. Lison, *Toxicol. Appl. Pharmacol.*, 2005, **207**, 221–231.

21 R. Murphy, J. N. Coleman, M. Cadek, B. McCarthy, M. Bent, A. Drury, R. C. Barklie and W. J. Blau, *J. Phys. Chem. B*, 2002, **106**, 3087–3091.

22 H. Athalin and S. Lefrant, *J. Raman Spectrosc.*, 2005, **36**, 400–408.

23 P. T. Lillehei, J. W. Kim, L. J. Gibbons and C. Park, *Nanotechnology*, 2009, **20**, 325708.

24 C. G. Salzmann, B. T. T. Chu, G. Tobias, S. A. Llewellyn and M. L. H. Green, *Carbon*, 2007, **45**, 907–912.

25 S. Attal, R. Thiruvengadathan and O. Regev, *Anal. Chem.*, 2006, **78**, 8098–8104.

26 H. Xia, Y. Wang, J. Lin and L. Lu, *Nanoscale Res. Lett.*, 2012, **7**, 33.

27 P. Xu, J. Loomis, B. King and B. Panchapakesan, *Nanotechnology*, 2012, **23**, 315706.

28 Y. K. Kim and H. Park, *Energy Environ. Sci.*, 2011, **4**, 685–694.

29 F. F. de Mul, *Monte Carlo simulation of Light transport in Turbid Media*, 2004.

30 F. F. de Mul, M. H. Koelink, M. L. Kok, P. J. Harmsma, J. Greve, R. Graaff and J. G. Aarnoudse, *Appl. Opt.*, 1995, **34**, 6595–6611.

31 F. De Nicola, C. Pintossi, F. Nanni, I. Cacciotti, M. Scarselli, G. Drera, S. Pagliara, L. Sangaletti, M. De Crescenzi and P. Castrucci, *Carbon*, 2015, **95**, 28–33.

32 Q. Li, B. J. Lee, Z. M. Zhang and D. W. Allen, *J. Biomed. Opt.*, 2008, **13**, 054064.

33 R. J. Nordstrom, F. Ayers, A. Grant, D. Kuo, D. J. Cuccia and A. J. Durkin, presented in part at the Design and Performance Validation of Phantoms Used in Conjunction with Optical Measurements of Tissue, 2008.

34 M. S. Dresselhaus, G. Dresselhaus, R. Saito and A. Jorio, *Phys. Rep.*, 2005, **409**, 47–99.

35 D. Cai, A. Neyer, R. Kuckuk and H. M. Heise, *J. Mol. Struct.*, 2010, **976**, 274–281.